Computational Characterization of a Photonic Crystal Cantilever Sensor Using a Hexagonal Dual-Nanoring-Based Channel Drop Filter

Bo Li, Fu-Li Hsiao, and Chengkuo Lee, *Member, IEEE*

***Abstract*—We investigated photonic crystal-based dual-nanoring (DNR) channel drop filters for nanomechanical sensor applications. The backward drop mechanism is explained by a proposed model. A resonant peak at 1553.6 nm with a quality factor better than 3800 is observed at the backward drop port. When this DNR is integrated at the junction between the silicon cantilever and the substrate, the deformation of the silicon cantilever can be detected in terms of the resonant wavelength and resonant wavelength shift. The derived minimum detectable force is 37 nN.**

***Index Terms*—Filter, photonic crystal (PhC), resonator, sensor.**

I. Introduction

MICRORING resonator device is a well-known approach to achieve channel drop filters of high quality [1]–[4]. One of the most promising designs is the strip-based microring resonator [4]–[6]. A circulating resonant mode of the ring resonator is excited by the coupled light in propagation along the main bus waveguide. The free spectral range (FSR) of the filter is desired to be larger than the optical communication wavelength range. The ring radius of a silicon ring waveguide is required to be less than 5 μm so that the FSR can be larger than 30 nm in the case of the C-band spectra range [4]. However, the bending loss of a dielectric waveguide increases substantially with the reduction of the ring radius. In addition, the performance of strip-based microring resonators is strongly affected by the surface roughness and the nanometer scale gap between the ring and the bus waveguide presents a grand challenge in manufacturing [7].

In 1987, photonic crystals (PhCs) were initially proposed by Yablonovitch [8] and John [9]. PhCs are artificially made materials of periodic dielectric nanostructures that can exhibit a photonic band gap (PBG) for certain frequency ranges [10]. The photons can be controlled arbitrarily by introducing defect modes within the PBG, e.g., point and line defects. The PBG effect of PhCs reveals highly confined and localized light. Many optical communication devices based on PhCs such as channel drop filters, power splitters, PhC coupler, and light sources are reported [11]–[15]. Particularly, the channel drop filter plays a key role in photonic integrated circuits (ICs) [15] because it integrates various functional elements, e.g., multiplexer [16], [17], switch [18], and directional coupler [19] together. Compared with conventional optical waveguide devices, PhC devices can perform the same function with their nanometric sizes, hence raising channel densities within a small chip of photonic ICs. Literatures of channel drop filters aimed to enhance the compactness, high spectral selectivity, wide spectral tunability, fast switching, and low-power switching have been reported [20]–[22]. The PhCs-based channel drop filters adapted in wavelength division multiplexer (WDM) communication systems have been reported as well [23]–[26]. An optical microring sensor integrated with a silicon microcantilever has also been investigated for force and strain sensing [27], while silicon microcantilevers using a single nanoring (SNR) as force and strain sensors have been reported recently [28]. In this study, three types of cantilevers integrated with a PhCs-based hexagonal dual-nanoring (DNR) channel drop filter are investigated as an optical nanomechanical sensor.

II. PhC Structure and DNR Resonator

A. Modeling Methodology

Fan *et al.* [11] reported channel drop filters based on 2-D PhCs of a square lattice. The resonators comprise one or two point defects inside the 2-D PhCs. The size and the refractive index of point defects are varied to match the desired resonance condition. The quality factors (Q-factors) of resonant peaks of forward and backward drop ports are reported as 1000 and 6000, respectively. Qiang *et al.* [24] reported a computational study of 2-D PhCs add-drop filters of the square lattice. Four additional scatters, i.e., small air holes, are placed at the four corners of the square-trace defect to form a square ring resonator. By adding the scatters, the Q-factor of the single and two square ring resonators is enhanced from 160 to over 1000, and to over 2000, respectively. The drop direction and wavelength are reported to be relevant to position between two rings.

PhCs-based ring resonators provide ultralow bending loss due to very good optical confinement. It offers a good alternative of

Manuscript received November 14, 2009; revised August 3, 2010; accepted September 12, 2010. Date of publication September 23, 2010; date of current version July 8, 2011. This work was supported in part by the University Research Committee (URC) Fund under Grant R-263-000-475-112 at the National University of Singapore, Singapore, and in part by A-STAR, Science and Engineering Research Council under Grant 0921010049. The review of this paper was arranged by Associate Editor E. T. Yu.

B. Li and C. Lee are with the Department of Electrical and Computer Engineering, National University of Singapore, 117576, Singapore (e-mail: g0900320@nus.edu.sg; elelc@nus.edu.sg).

F.-L. Hsiao is with the Graduate Institute of Photonics, National Changhua University of Education, Changhua City, Taiwan (e-mail: fulihsiao@gmail.com).

Color versions of one or more of the figures in this paper are available online at http://ieeexplore.ieee.org.

Digital Object Identifier 10.1109/TNANO.2010.2079942

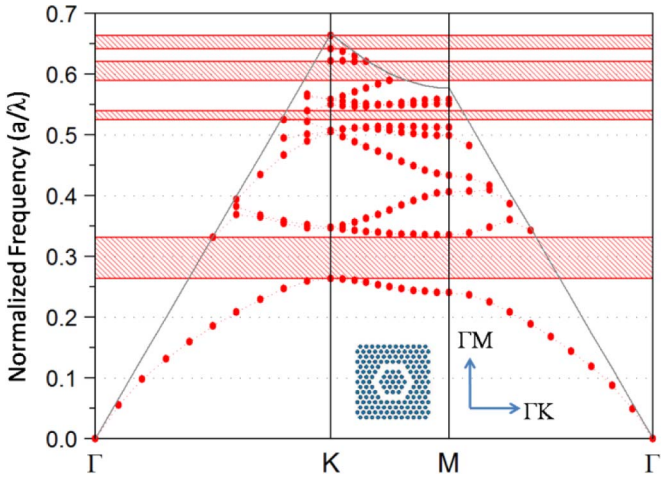

Fig. 1. Band structure of the PhC structure of the hexagonal lattice.

ultracompact resonators with a high Q-factor and high wavelength selectivity in contrast to present microring resonators with the challenges mentioned previously.

We investigated PhCs-based channel drop filters of a hexagonal lattice, i.e., hexagonal nanoring resonator filters without scatters, in this computational study. On the other hand, Kitamura *et al.* reported that the cavity modes obtained by the plane wave expansion (PWE) method in the PhC-slab structure are in good agreement with the measured results [29]. By using this PWE method, the band structure of a silicon PhC slab with the hexagonal lattice of air holes is derived and shown in Fig. 1. A silicon PhC slab of 220 nm thickness is released from a silicon-on-insulator (SOI) substrate, where the refractive index of air/220 nm-Si/air is derived as 1, 3.46, and 1, respectively. According to the derived band gap map in Fig. 1, the normalized frequency range of the first photonic band gap extends from 0.26 to 0.33 in the TM polarization electromagnetic wave, i.e., the magnetic field parallel to the surface of the silicon slab. The ratio between the radius of air holes (r) and lattice constant (a) is selected as 0.292, the center of the band gap range. The corresponding directions of ΓM and ΓK with respect to the hexagonal lattice are indicated in the inset of Fig. 1. The corresponding band gap wavelength range extends from 1.242 μm to 1.577 μm. A combinational approach of the 2-D finite-difference time-domain (FDTD) method and the effective refractive index (ERI) approximation was deployed to calculate and predict the performance of the channel drop filter and the filed distribution of resonant mode in this study. Qiu reported a good agreement between the data derived by this combinational approach and the full vector three-dimensional (3-D) FDTD method [30]. Furthermore, experimental data have been predicted well by this combinational approach by the other groups as well [31], [32]. As shown in the inset of Fig. 1, a hexagonal nanoring is formed by removing air holes of hexagonal trace in the 220-nm-thick silicon PhC slab. The resonance frequency of the nanoring resonator is derived as 1553.6 nm. The ERI of the 220-nm silicon slab is 2.7967 in the simulation. The hexagonal lattice gives the nanoring resonator a better photon confinement such that a high Q-factor is achieved [33], [34].

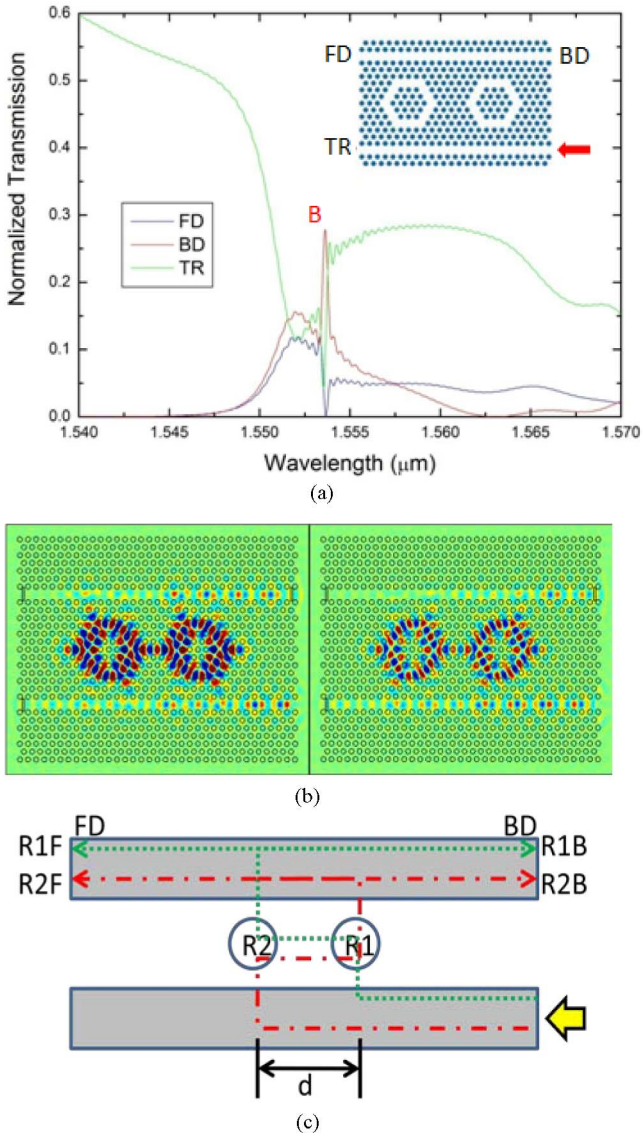

Fig. 2. (a) Spectra of ports FD, BD, and TR for the DNR channel drop filter. (b) No-load case: out-of-plane magnetic field distribution plot at resonant steady state. (c) Conceptual drawing of light paths dropped through DNR resonators to the FD and BD ports.

A DNR resonator is depicted in the inset of Fig. 2(a). Two nanorings are sandwiched in between two bus waveguides. The input port is indicated by a red arrow, while the corresponding spectra of forward drop (FD), transmission (TR), and backward drop (BD) ports are denoted by blue, green, and red curves, respectively. The distance between the center of the left nanoring and that of the right nanoring is named as the center-to-center nanoring distance, and it is $11a$ in Fig. 2(a). A resonant peak with a Q-factor of 3884 is observed at 1553.6 nm in the BD port, i.e., marked with B. The spectra of both FD and TR reveal a dip at this wavelength. At this wavelength, the light intensity at the FD port is only 8% of the peak intensity at the BD port. It means that a resonant field distribution leads to a good backward drop condition.

B. Channel Drop Mechanism

Fig. 2(b) shows frames of the resonator's magnetic-field distribution in the steady-state condition which is varying with time. The TM mode Gaussian beam centered at the resonant wavelength is launched into the resonator from the bottom-right input port of each structure. We define the right-hand side ring as R1 and the left-hand side ring as R2. The input light beam comes from the bottom-right side and travels along the input waveguide and excites the nanoring region. The nanorings then couple the light energy of a certain wavelength to the output waveguide. The field distribution graphs show that the two rings are always in the same phase, and the light energy strength changes periodically and simultaneously. A strong field is observed from the input waveguide to both nanorings and the middle four holes between the two nanorings. A strong coupling effect between rings and the drop waveguide can be obtained too. However, only the BD signal is active. A high level of energy exchange in the middle four holes between the DNR indicates that the two rings are not working independently of each other. Light coming from the input waveguide will travel within the two rings first before coupling to the drop port at the output waveguide.

Fig. 2(c) shows a proposed light drop mechanism in a DNR resonator-based channel drop filter. The input light comes from the right-bottom side of the waveguide. The circles R1 and R2 indicate the two nanorings. The center-to-center nanoring distance between the DNR is denoted by d. The light coupled and propagated mainly to the FD and BD ports via R1 and is denoted as R1F and R1B, respectively. Again, R2F and R2B refer to the light mainly coupled and propagated to the FD and BD ports via R2. When the light of R1B and R2B is in phase and the light of R1F and R2F is out of phase, constructive and deconstructive interference occurs between R1B, R2B, and R1F, R2F, respectively. Therefore, 100% of dropped light goes to the BD port, i.e., the total backward drop condition, due to the conservation of energy. On the other hand, if R1 and R2 resonate independently, a total constructive interference will occur between R1F and R2F because the phase difference between them is zero for an arbitrary d value.

In Fig. 2(a), the observed strong resonant peak in the BD port implies that the resonances of the two nanorings are not independent. Besides, obvious coupling effects are observed between the two nanorings via the nearest two vertices in Fig. 2(b). The light path difference between R1B and R2B is zero since both distances are waveguide length plus d. Hence, there is no phase difference between R1B and R2B, satisfying the first condition. The light path of R2F is $2d$ longer than R1F. The second condition, i.e., the deconstructive interference occurring between R1F and R2F, can be achieved by having d complied with the relation $k{\cdot}d = n\pi + \pi/2$, where k is the wave vector of the guided mode and n is an integer; hence, $d = n{\cdot}\lambda/4$, where λ is the guided mode wavelength. The corresponding guided mode wavelength of the DNR resonator of our PhC slab is about 1553.6 nm, which is derived by PWE method. The nanoring's center-to-center distance is 11a in Fig. 2(a), i.e., 4510 nm. It is very close to $12{\cdot}(\lambda/4)$ for λ of 1553.6 nm. Thus, the second condition is satisfied as well. As a result, the two rings of the DNR behave as a resonator. The drop mechanism obeys the field distribution symmetry theory discussed by Fan *et al.* [11]. We have computationally proved that the DNR is a good backward drop channel filter of high drop efficiency in the configuration as shown in Fig. 2(a), while the center-to-center distance between the two rings of the proposed DNR is found to have strong influence on the channel drop behavior.

III. Operation Mechanism of the PhC Cantilever Sensor

Based on the drop mechanism of the DNR resonator, the size of the ring and the separation distance of the DNR have great effect on the resonant wavelength. These properties of the DNR make it suitable to be used as a sensing element for force and strain detection since the resonant wavelength measured at the BD port is strongly dependent on the ring size and separation distance. When the DNR is deformed, the resonant wavelength will change accordingly. Hence, the DNR resonator can be placed at the junction of a free-standing silicon cantilever and an edge of substrate as shown in Fig. 3(a). When an external force is applied on the cantilever free end, strain at the junction is created. Such strain is in linear proportion to the applied force. More precisely, the vertical displacement (Z-displacement) at different positions along the longitudinal direction of the cantilever gradually increases as the position moves to the cantilever edge under an applied force. The Z-displacement at a particular position linearly increases in proportion to the increasing loading force. The cantilever of length 50 μm and width 15 μm can be patterned and released from the 220-nm-thick silicon device layer of a SOI substrate. The lattice constant (a) of 410 nm and air-hole radius (r) of 180 nm of the PhC slab of the hexagonal lattice are deployed in modeling. Two hexagonal nanorings are placed along the longitudinal direction of the cantilever and are separated by four air holes in their symmetric axis. The whole layout configuration including the lattice constant a, air-hole radius r, and the air-hole separation between waveguides and rings has been optimized in order to achieve the resonant peak of higher Q-factor at the BD port.

By leveraging this unique feature, the input and output ports of the DNR resonator are arranged on the same side of the cantilever sensor as shown in Fig. 3(a). It renders a simple configuration of a cantilever sensor with advantage of an easy setup of resonator wavelength measurement with respect to the optical fiber alignment task. To optimize the performance of the DNR in terms of a sensing element for the cantilever sensor, three types of cantilever sensors are proposed in Fig. 3(b). The junction of the cantilever and the edge of the substrate is placed at the right corner of the first ring (R1), i.e., the type 1 cantilever. The junction of the cantilever and the edge of the substrate is placed at the left corner of the R1 for the type 2 cantilever, and is arranged at the right corner of the second ring (R2) for the type 3 cantilever, respectively.

In the applications, either external force or surface stress will introduce a vertical displacement at the cantilever end and strain at the DNR resonator sensing element region. Finite element

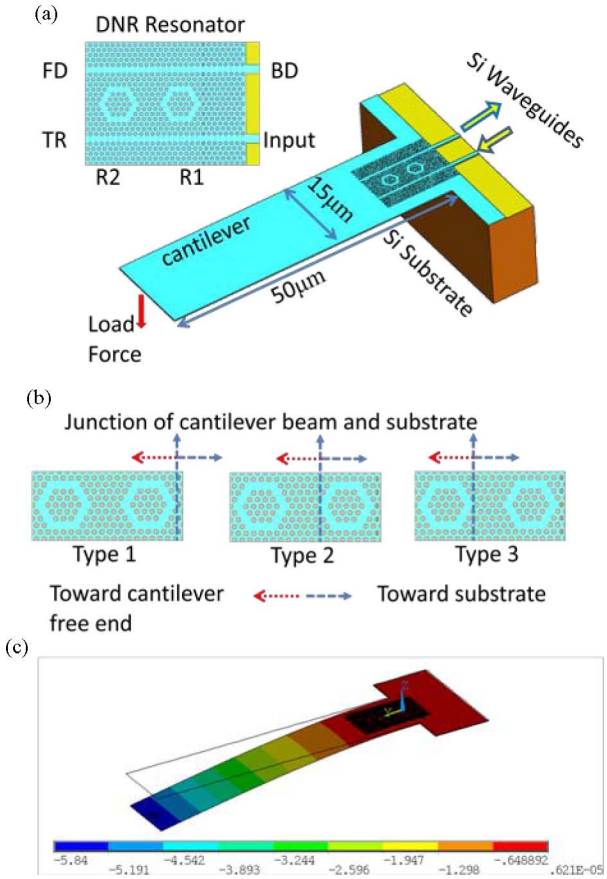

Fig. 3. (a) 3-D illustration of the PhC cantilever sensor using the hexagonal DNR resonator. (b) Three types of cantilever sensors with different locations of the DNR resonator around the junction of the cantilever and substrate. (c) Side view of FEA simulation result of the vertical displacement along the cantilever sensor using the DNR when there is 0.2 μN force applied at the end of cantilever.

analysis (FEA) is deployed to obtain the deformation data of holes in the PhC air-hole array under various loading forces applied at the center point of the cantilever free end, as shown in Fig. 3(c). The Young's modulus and Poisson's ratio of Si used in FEA simulation is 130 GPa and 0.3, respectively. The FEA simulation results show that the location of DNR resonators can lead to different strain and deformation for all the three types of cantilevers. We further applied the numerical 2-D FDTD method to simulate the propagation of the electromagnetic waves in the deformed PhC DNR resonator structure in the presence of various applied force loads. We expect the resonant peak at the BD port will vary according to the strain of the DNR resonator. In our previous study [35], we realized that the shape change of the air holes in the deformed PhC structure does not affect the output resonant behavior. More importantly, the relative position shift of these air holes in the deformed PhC structure plays a major role in contribution to the resonant behavior. Thus, we recorded the position of holes in the deformed region of the cantilever under force load according to the FEA results, and conducted the 2-D FDTD modeling based on the layout of such deformed DNR resonators.

IV. Characteristics of Cantilever Sensors

In the current study, the DNR resonator contains two nanorings and four-hole separation between the two nanorings, i.e., the 11a of the center-to-center nanoring distance between the DNR. Therefore, the resonant behavior is expected to be affected by ring deformation and strain in the four-hole separation. Due to different locations of DNR resonator in three cantilevers, we can investigate the resonant behavior with respect to ring deformation and strain in the four-hole separation. Fig. 4(a)–(c) shows the resonant wavelength peak derived at the BD port under various force loads with a step of 0.1 μN for all the three cantilevers. The resonant peak at 1553.6 nm with a Q-factor of about 3800 for the no-load case is the same for all of three cantilevers. The spectra plot of the BD port shows the shapes and the locations of the gradually changed resonant peak. Shapes of the resonant peak give us information about the peak quality. Moreover, we can further imply the actual behaviors of the propagating light inside the PhC structure. We defined the resonant peak shift as the wavelength difference between the new peak under force load and the original peak of the no-load case. The resonant wavelength will shift to the higher wavelength as the load force increases, i.e., a red shift, in all the three cases. For the type 1 cantilever [Fig. 4(a)], the resonant peak shifts from 1553.6 nm to 1554.9 nm with the same Q-factor when the load force changes from 0 to 0.4 μN. However, as the loading force approaches to 0.5 μN, the output signal intensity at the BD port becomes relatively low in comparison to the other cases of smaller force loads, while the FD signal shows comparable intensity as the BD signal. Major portion of the input energy does not couple into the BD and FD ports. Thus, we observed strong output intensity at the TR port. It refers to the resonant behavior for the BD is degraded due to the deformed DNR resonator.

On the other hand, for the type 2 cantilever [Fig. 4(b)], the left nanoring (R2) and the four-hole separation will experience deformation under force loads, while the equivalent deformation within the R2 region in the type 2 cantilever is expected to be smaller than such deformation of the R2 in the case of the type 1 cantilever. The resonant behavior maintains the channel drop mechanism up to the load force of 0.7 μN. The BD behavior is degraded in the case of higher force load. Fig. 4(c) shows the output resonant peaks at the BD port for various force loads in type 3 cantilevers. In this case, only R2 is kept within the deformation range. Since the shape of the right nanoring (R1) and the four-hole separation are maintained as the same as the no-load case, the deformation of R2 provides the largest detectable force range from 0 to 1 μN. In other words, the BD behavior is degraded in the case of force load higher than 1 μN. However, it also implies that the type 3 cantilever becomes less sensitive due to the smaller portion of the DNR resonator maintained within the deformation region, i.e., less strain experienced.

Fig. 5(a) illustrates that the relationship between the resonant peak wavelength versus Z-displacement and applied force at the cantilever end, and the relevant data are depicted in Fig. 5(b). We observed a good linear relationship of the resonant peak wavelength versus applied force as well as the Z-displacement for the type 1 cantilever in Fig. 5(a). The slope of linear data of the type

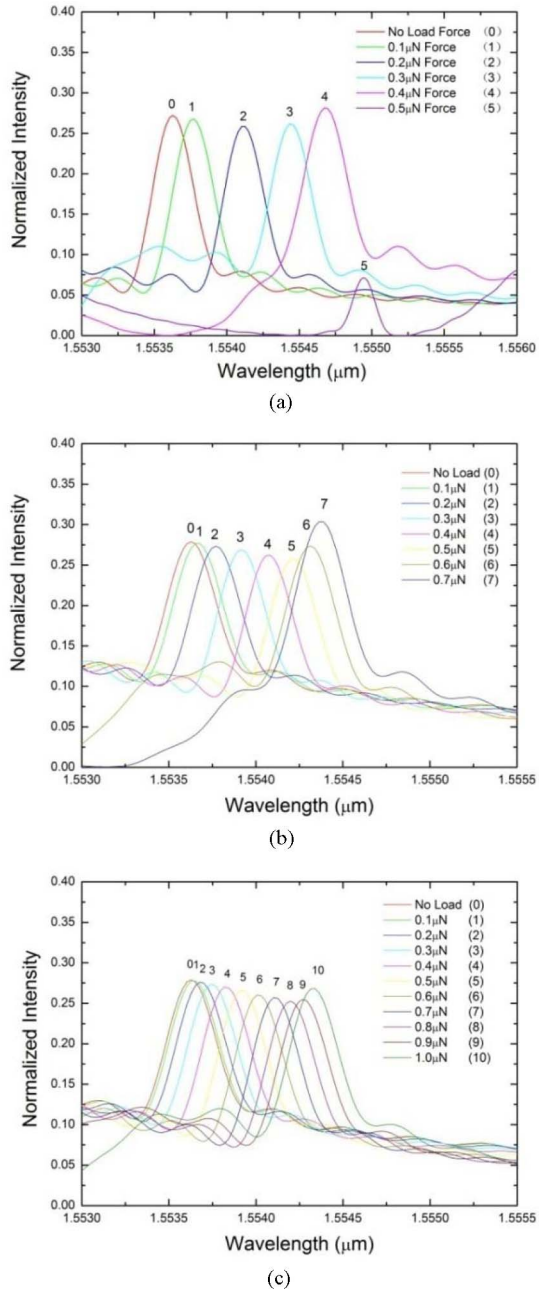

Fig. 4. Resonant wavelength peak at the backward drop (BD) port under various force loads: (a) type 1 cantilever; (b) type 2 cantilever; (c) type 3 cantilever.

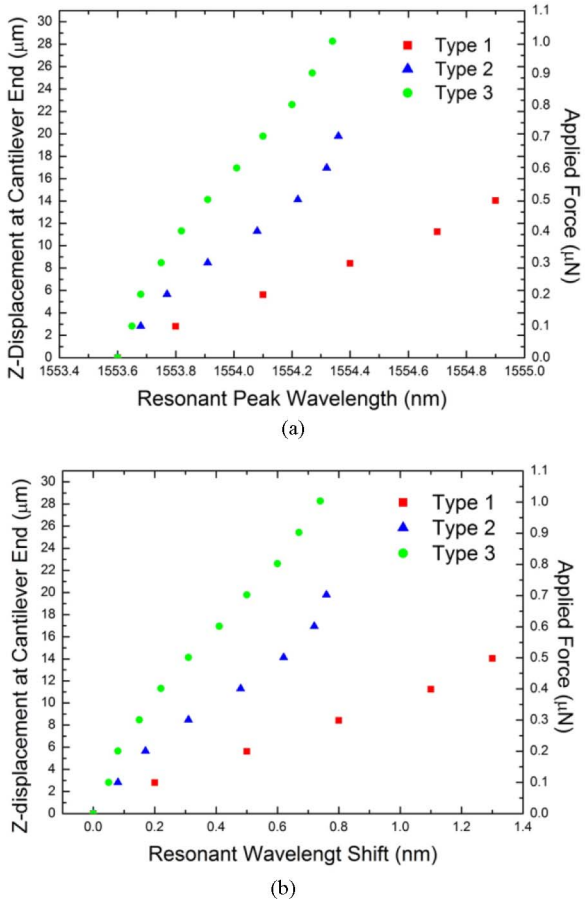

Fig. 5. (a) Resonant wavelength as functions of the *Z*-displacement and applied force for three types of cantilevers. (b) Resonant wavelength shift as functions of the *Z*-displacement and the applied force for three types of cantilevers.

1 cantilever is derived as 370 nN/nm (applied force/wavelength shift) and 10.30 μm/nm (*Z*-displacement/wavelength shift) in Fig. 5(b). It is suggested that the minimum detectable force and minimum detectable displacement will be 37 nN and 1.03 μm, respectively, if the wavelength detection resolution is 0.1 nm for the testing setups [35].

Second, the data points of type 2 and type 3 cantilevers follow approximately linear behavior in both figures. The slope of data fitting lines in Fig. 5(b) is derived as 830 nN/nm or 23.26 μm/nm for the type 2 cantilever, and 1250 nN/nm or 35.57 μm/nm for the type 2 cantilever, respectively. Therefore, the minimum detectable force and the minimum detectable displacement are derived as 83 nN and 2.33 μm for the type 2 cantilever, and 125 nN and 3.56 μm for the type 3 cantilever, respectively. It implies that the type 1 cantilever is more sensitive than the other two types but having the smallest detectable force range, i.e., less than 0.5 μN. In the case of the type 3 cantilever, the detectable force range is up to 1 μN, although the minimum detectable force is 125 nN. Compared with the nanocavity resonator cantilever and the SNR resonator cantilever, the proposed type 1 DNR cantilever achieves better data of the minimum detectable force [28], [35].

For the type 3 cantilever, the linearity looks less perfect than the other two cases. This can perhaps be attributable to the presence of only a nanoring located within the deformation range. To further clarify the origin of dependence of resonant wavelength versus force loads in the SNR resonator, we conducted the 2-D FDTD modeling for a cantilever with an SNR at the position as the same as the case of the type 3 cantilever. Fig. 6 illustrates the dependence of resonant wavelength on force loads, and the resonant wavelength shift on force loads for the cantilever of the SNR resonator and the type 3 cantilever. Without having the coupling effect with another nanoring, the data of the cantilever with SNR follow a second-order polynomial curve. In

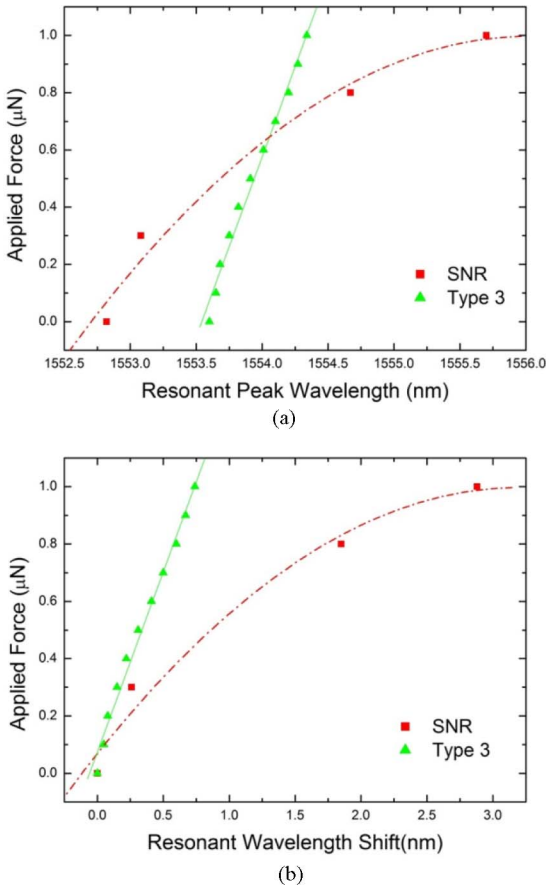

Fig. 6. (a) Curve of the resonant wavelength versus applied force for the cantilever of SNR and type 3 cantilever. (b) Curve of the resonant wavelength shift versus applied force for the cantilever of SNR and type 3 cantilever.

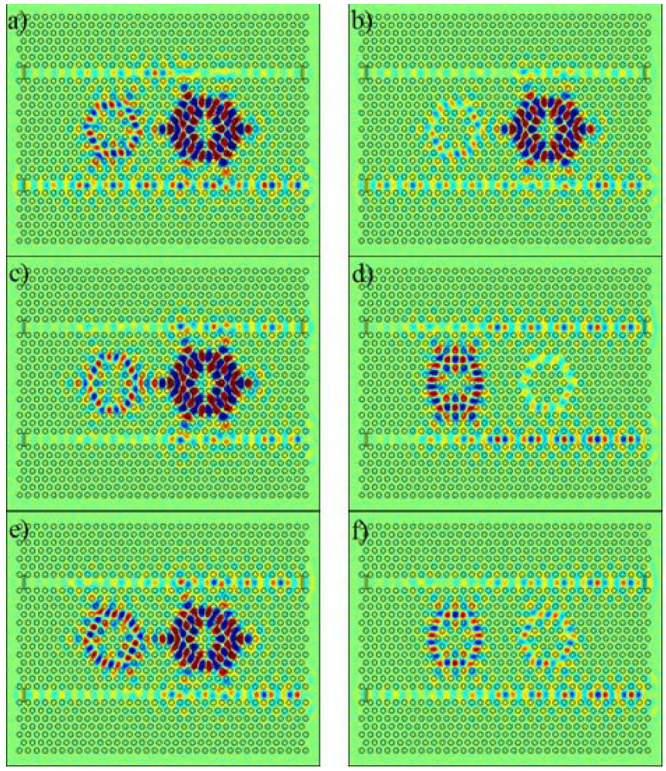

Fig. 7. Images of continuous the wave field distribution for DNR resonators under deformation: (a) and (b) refer to the type 1 cantilever under 0.5 μN force; (c) and (d) refer to the type 2 cantilever under 0.7 μN force; (e) and (f) refer to the type 3 cantilever under 1 μN force.

contrast to this second-order polynomial data, a relatively linear fitting line is given for data derived for the type 3 cantilever. We conclude the linear relationship between the resonant wavelength and applied force or the *Z*-displacement is obtained for the cantilevers using the DNR resonator, while same linear data are derived for the resonant wavelength shift as well. Linearity is observed for the type 3 cantilever because of that only R2 experienced the deformation. The resonant behavior is still dominant by the DNR configuration. Thus, data of the type 3 cantilever keep the linearity.

V. Continuous Wave Simulation

As we discussed earlier, the total backward drop occurs at the device configuration that fulfills two conditions. Firstly, deconstructive interference occurs between R1F and R2F. Secondly, constructive interference occurs between R1B and R2B. With the observed data in Figs. 5 and 6, it is very interesting to us that the different origin of the resonant mechanism for three types of cantilevers under deformation.

Thus, a continuous wave field distribution has been established on the DNR resonator under the maximum applied force within the detectable force range for the three cantilevers, as shown in the Fig. 7. The field distribution plot follows the same procedure as we conducted for the DNR of the no-load condition [Fig. 2(b)]. Fig. 7(a) and (b) illustrates the case of the type 1 cantilever deformed under 0.5 μN constant force. In this case, although the field is strong in the ring resonator region, very little energy could couple over to the output waveguide ports. Most of the energy is coupled back to the input waveguide and eventually propagates to the TR port. Such scenario fits quite well with the observation in the spectrum. From Fig. 4(a), we observed that the BD port lost most of its energy in comparison to the other cases of the lower applied force. The intensity ratio of the BD signal over the TR signal is 1/4 in this case. The DNR resonator loses its channel drop effect because of the deformed ring shape and the distance change of the four-hole separation, as well as the deviated condition of the symmetric coupling condition between the two rings. Therefore, the two conditions for the backward channel drop are no longer fulfilled. R1 has a stronger field as compared with R2, which is different from the no-load case, as shown in Fig. 2(b). Moreover, R1 and R2 show circulating light of a bit out-of-phase for each other and minor coupling occurs between two nanorings due to the deformed DNR resonator. Thus, deconstructive interference occurs in the output waveguide and the only limited energy is coupled to the BD port as well as FD port.

For the type 2 cantilever, R1 and R2 are totally out-of-phase with each other, as shown in Fig. 7(c) and (d). R1 and R2 are working dominantly in different time intervals, respectively. R1 resonation is dominant in the case shown in Fig. 7(c). Strong coupling occurs between the two rings and most energy in the

output waveguide comes only from R1. R2 becomes the dominant nanoring in resonance and there is no energy exchange between two nanorings in the case shown in Fig. 7(d). The energy coupled into the output waveguide is mostly contributed by R2. Fig. 7(e) and (f) illustrates the continuous wave field distribution for the type 3 cantilever under deformation. It is similar with the results of the type 2 case. The two nanorings show resonance in different time intervals and only one nanoring is activated in a period of time. However, the energy condition of R2 in the type 3 cantilever under 1 μN force does not change with the different modes. The same level of energy is always observed in R2 and this is mainly because only R2 is located in the deformed region. In other words, as R2 is located in the cantilever region which is under deformation, the level of energy observed in R2 remains the same. In summary, we observed that the continuous wave field distributed between the two nanorings provides evidence to explain the derived backward channel drop behavior.

VI. Conclusion

In this study, we proposed a PhC-based DNR resonator with significant backward drop function. We also explored the feasibility of using such DNR resonators as channel drop filters for a nanomechanical cantilever sensor application. By investigating the location of the DNR resonator, we optimized the design of the DNR cantilever sensor. The resonant peak with the Q-factor of about 3800 and minimum detectable force of 37 nN are derived. Linear curves are obtained for the resonant wavelength and the resonant wavelength shift versus the applied force or vertical displacement. The resonant mechanism is contributed by both of the nanorings and the separation between two nanorings. The simulation of continuous wave field distribution provides evidence of the resonant behavior of the DNR resonator. This unique nanomechanical cantilever sensor is promising in applications such as force sensing and detection of displacement.

Acknowledgment

The authors would like to thank Prof. G. Liang and Prof. A. Danner for their valuable advice, and also grateful to the staff at the Centre for Integrated Circuit Failure Analysis and Reliability (CICFAR), Centre for Optoelectronics and Computational Nanoelectronics and Nanodevices Laboratory of National University of Singapore for technical support.

References

[1] D. G. Rabus, M. Hamacher, U. Troppenz, and H. Heidrich, "High-Q channel-dropping filters using ring resonators with integrated SOAs," *IEEE Photon. Technol. Lett.*, vol. 14, no. 10, pp. 1442–1444, Oct. 2002.

[2] A. Melloni, R. Costa, P. Monguzzi, and M. Martinelli, "Ring-resonator filters in silicon oxynitride technology for dense wavelength-division multiplexing systems," *Opt. Lett.*, vol. 28, pp. 1567–1569, 2003.

[3] T. Barwicz, M. A. Popovic, P. T. Rakich, M. R. Watts, H. A. Haus, E. P. Ippen, and H. I. Smith, "Microring-resonator-based add-drop filters in SiN:fabrication and analysis," *Opt. Exp.*, vol. 12, pp. 1437–1442, 2004.

[4] B. E. Little, J. Foresi, G. Steinmeyer, E. R. Thoen, S. T. Chu, H. Haus, E. Ippen, L. C. Kimberling, and W. Greene, "Ultra-compact Si-SiO_2 microring resonator optical channel dropping filters," *IEEE Photon. Technol. Lett.*, vol. 10, no. 4, pp. 549–551, Apr. 1998.

[5] V. R. Almeida, C. A. Barrios, R. R. Panepucci, and M. Lipson, "All optical control of light on a silicon chip," *Nature*, vol. 431, pp. 1081–1084, 2004.

[6] G. N. Nielson, D. Seneviratne, F. Lopez-Royo, P. T. Rakich, Y. Avrahami, M. R. Watts, H. A. Haus, H. L. Tuller, and G. Barbastathis, "Integrated wavelength-selective optical MEMS switching using ring resonator filters," *IEEE Photon. Technol. Lett.*, vol. 17, no. 6, pp. 1190–1192, Jun. 2005.

[7] B. E. Little, J. P. Laine, and S. T. Chu, "Surface-roughness-induced contradirectional coupling in ring and disk resonators," *Opt. Lett.*, vol. 22, pp. 4–6, 1997.

[8] E. Yablonovitch, "Inhibited spontaneous emission in solid-state physics electronics," *Phys. Rev. Lett.*, vol. 58, pp. 2059–2062, 1987.

[9] S. John, "Strong localization of phonics in certain disordered dielectric superlattices," *Phys. Rev. Lett.*, vol. 58, pp. 2486–2489, 1987.

[10] S. G. Johnson and J. D. Joannopoulos, "Designing synthetic optical media: Photonic crystals," *Acta Mater.*, vol. 51, pp. 5823–5835, 2003.

[11] S. Fan, P. R. Villeneuve, J. D. Joannopoulos, and H. A. Haus, "Channel drop filters in photonic crystals," *Opt. Exp.*, vol. 3, pp. 4–11, 1998.

[12] C. C. Chen, H. D. Chien, and P. G. Luan, "Photonic crystal beam splitters," *Appl. Opt.*, vol. 43, pp. 6188–6190, 2004.

[13] H.-T. Chien, C. Lee, H.-K. Chiu, K.-C. Hsu, C.-C. Chen, J. A. Ho, and C. Chou, "The comparison between the graded photonic crystal coupler and various couplers," *IEEE J. Lightw. Technol.*, vol. 27, no. 7, pp. 2570–2574, Jul. 2009.

[14] L. M. Chang, C. H. Hou, Y. C. Ting, C. C. Chen, C. L. Hsu, J. Y. Chang, C. C. Lee, G. T. Chen, and J. I. Chyi, "Laser emission from GaN photonic crystals," *Appl. Phys. Lett.*, vol. 89, pp. 1116–1118, 2006.

[15] S. Kim, I. Park, and H. Lim, "Highly efficient photonic crystal-based multi-channel drop filters of three-port system with reflection feedback," *Opt. Exp.*, vol. 12, pp. 5518–5525, 2004.

[16] K. H. Hwang and G. H. Song, "Design of a high-Q channel-drop multiplexer based on the two-dimensional photonic-crystal membrane structure," *Opt. Exp.*, vol. 13, pp. 1948–1957, 2005.

[17] D. S. Park, B. H. O, S. G. Park, E. H. Lee, and S. G. Lee, "Photonic crystal-based GE-PON triplexer using point defects," *Proc. SPIE*, vol. 6897, pp. 689711-1–689711-9, Feb. 2008.

[18] E. A. Camargo, H. M. H. Chong, and R. M. De La Rue, "2-D photonic crystal thermo-optic switch based on AlGaAs/GaAs epitaxial structure," *Opt. Exp.*, vol. 12, pp. 588–592, 2004.

[19] Y. D. Wu, M. L. Huang, and T. T. Shih, "Optical interleavers based on two-dimensional photonic crystals," *Appl. Opt.*, vol. 46, pp. 7212–7217, 2007.

[20] M. Lipson, "Guiding, modulating and emitting light on silicon—Challenges and opportunities," *IEEE J. Lightw. Technol.*, vol. 23, no. 12, pp. 4222–4238, Dec. 2005.

[21] M. Notomi, A. Shinya, S. Mitsugi, E. Kuramochi, and H. Y. Ryu, "Waveguides, resonators and their coupled elements in photonic crystal slabs," *Opt. Exp.*, vol. 12, pp. 1551–1561, 2004.

[22] B. E. Little, S. T. Chu, H. A. Haus, J. Foresi, and J. P. Laine, "Microring resonator channel dropping filters," *J. Lightw. Technol.*, vol. 15, pp. 998–1005, 1997.

[23] D. Goldring, U. Levy, and D. Mendlovic, "Highly dispersive microring resonator based on one dimensional photonic crystal waveguide design an analysis," *Opt. Exp.*, vol. 15, pp. 3156–3168, 2007.

[24] Z. Qiang, W. Zhou, and R. A. Soref, "Optical add-drop filters based on photonic crystal ring resonators," *Opt. Exp.*, vol. 15, pp. 1823–1831, 2007.

[25] F. Monifi, A. Ghaffari, M. Djavid, and M. S. Abrishamian, "Three output port channel-drop filter based on photonic crystals," *Appl. Opt.*, vol. 48, pp. 804–809, 2009.

[26] Z. Zhang and M. Qiu, "Compact in-plane channel drop filter design using a single cavity with two degenerate modes in 2-D photonic crystal slabs," *Opt. Exp.*, vol. 13, pp. 2596–2604, 2005.

[27] I. Kiyat, C. Kocabas, and A. Aydinli, "Integrated microring resonator displacement sensor for scanning probe microscopies," *J. Micromech. Microeng.*, vol. 14, pp. 374–381, 2004.

[28] T. T. Mai, F.-L. Hsiao, C. Lee, W. Xiang, C .-C. Chen, and W. K. Choi, "Optimization and comparison of photonic crystal resonators for silicon microcantilever sensors," *Sens. Actuators A*, to be published.

[29] M. Kitamura, S. Iwamoto, and Y. Arakawa, "Enhanced light emission from an organic photonic crystal with a nanocavity," *Appl. Phys. Lett.*, vol. 87, pp. 151119-1–151119-3, 2005.

[30] M. Qiu, "Effective index method for the heterostructure-slab-waveguides-based two-dimensional photonic crystals," *Appl. Phys. Lett.*, vol. 81, pp. 1163-1–1163-3, 2002.

[31] W. Zheng, M. Xing, G. Ren, S. G. Johnson, W. Zhou, W. Chen, and L. Chen, "Integration of a photonic crystal polarization beam splitter and waveguide bend," *Opt. Exp.*, vol. 17, pp. 8657–8668, 2009.
[32] Y. Chassagneux, R. Colombelli, W. Maineults, S. Barbieri, S. P. Khanna, E. H. Linfield, and A. G. Davies, "Predictable surface emission patterns in terahertz photonic-crystal quantum cascade lasers," *Opt. Exp.*, vol. 17, pp. 9492–9502, 2009.
[33] A. D'Orazio, M. De Sario, V. Marrocco, V. Petruzzelli, and F. Prudenzano, "Photonic crystal drop filter exploiting resonant cavity configuration," *IEEE Trans Nanotechnol.*, vol. 7, no. 1, pp. 10–13, Jan. 2008.
[34] F.-L. Hsiao and C. Lee, "Computational study of photonic crystals nanoring resonator for biochemical sensing," *IEEE Sens. J.*, vol. 10, no. 7, pp. 1185–1191, Jul. 2010.
[35] C. Lee, R. Radhakrishnan, C.-C. Chen, J. Li, J. Thillaigovindan, and N. Balasubramanian, "Design and modeling of a nanomechanical sensor using silicon photonic crystal," *IEEE J. Lightw. Technol.*, vol. 26, no. 7, pp. 839–846, Apr. 2008.

Bo Li received the B.Sc. degree from the Department of Electrical and Computer Engineering, National University of Singapore, Singapore, in 2009, where he is currently working toward the Ph.D. degree.

Fu-Li Hsiao received the B.S. degree from the Department of Physics, National Changhua University of Education, Changhua City, Taiwan, in 2002, and the Ph.D. degree from FEMTO-ST of University of Franche-Comte, Besançon, France, and from the Department of Optics and Photonics, National Central University, Jhongli City, Taiwan, in 2008.

He was a Research Fellow at the Department of Electrical and Computer Engineering, National University of Singapore, from 2008 to 2009. He is currently an Assistant Professor in the Graduate Institute of Photonics, National Changhua University of Education,. His current research interests include photonic crystals, phononic crystals, and optical MEMS.

Chengkuo Lee (S'93–M'96) received the M.S. degree in materials science and engineering from National Tsing Hua University, Hsinchu, Taiwan, in 1991, the M.S. degree in industrial and system engineering from Rutgers University, New Brunswick, NJ, in 1993, and the Ph.D. degree in precision engineering from the University of Tokyo, Tokyo, Japan, in 1996.

He was a Foreign Researcher in the Nanometer-scale Manufacturing Science Laboratory, Research Center for Advanced Science and Technology, University of Tokyo, from 1993 to 1996. He was a JST Research Fellow in Mechanical Engineering Laboratory, National Institute of Advanced Industrial Science and Technology, Ministry of International Trade and Industry, Japan, in 1996. Thereafter, he was a Senior Research Staff Member at Microsystems Laboratory, Industrial Technology Research Institute, Hsinchu, Taiwan. He joined the Metrodyne Microsystem Corporation, Hsinchu, Taiwan, and established the MEMS device division and the first micromachining fab for commercial purpose in Taiwan, in 1997. He was a Manager of MEMS Device Division between 1997 and 2000. He was appointed as Adjunt Assistant Professor in the Department of Electrophysics in National Chiao Tung University, in 1998, and was the Adjunct Assistant Professor in Institute of Precision Engineering, National Chung Hsing University, from 2001 to 2005. He cofounded the Asia Pacific Microsystems, Inc. (APM) Hsinchu, Taiwan, in. 2001, and was the Vice President (VP) of R&D at the beginning, then became the VP of Optical Communication Business Unit and Special Assistant of CEO in charge of international business and technical marketing for MEMS foundry service at APM, Inc., till 2005. He was a Senior Technical Staff Member at the Institute of Microelectronics, A∗Star, Singapore. He has been an Assistant Professor at the Department of Electrical and Computer Engineering, National University of Singapore, Singapore, since 2005. He is the coauthor of a book titled *Advanced MEMS Packaging* (McGraw-Hill, 2010).

Dr. Lee has contributed more than 120 international conference papers and extended abstracts, 70 peer-reviewed international journal articles, and eight U.S. patents in MEMS, nanophotonics and nanotechnology fields. He is a member of the MRS and IEE Japan.